Developing a Simulator for Multispectral Optoacoustic Tomography

Efthymios Maneas, Stratis Tzoumas, Vasilis Ntziachristos and George Spyrou

***Abstract*— The aim of this study was the development of a simulator for Multispectral Optoacoustic Tomography (MSOT). The modelling pathway of the simulator was separated into the optical, the acoustic and the reconstruction part in generating finally a photoacoustic image. In this paper, the presented simulation geometry was based on a recently developed MSOT imaging system, but it can be easily modified to other imaging geometries. Through comparison between experimental and simulated data, a validation of the model as well as its limitations, perspectives and modifications are presented.**

I. INTRODUCTION

Photoacoustic (referred also as optoacoustic) imaging of biological tissues has a rapid growth of development in the last decade, mainly for resolving contrast of highly absorbing tissue components or contrast agents [1]-[5]. This technique is based on the photoacoustic phenomenon, i.e. the production of broadband ultrasonic waves via thermoelastic expansion caused by absorption of pulsed laser light irradiation. An improved approach of this technique, the Multispectral Optoacoustic Tomography [6], provides enhanced functional and molecular imaging capabilities demonstrated in a number of biomedical applications [7],[8].

The different proposed optoacoustic imaging modalities vary in performance and detectability characteristics, as well as in the reconstructed optoacoustic image. They can be also influenced by a number of factors including the tissue composition and its optical, thermal and acoustic properties, the light source and the ultrasound detector characteristics and their position to the imaging geometry. Also, an important role to the imaging formation plays the selected image reconstruction algorithm.

Simulation of MSOT can provide an accurate estimation of the contribution of these parameters in the final reconstructed optoacoustic image, acting also as a tool to optimize the whole imaging chain [11]. As mentioned before, an MSOT image is the result of the combination of certain optical and acoustic phenomena. Monte Carlo (MC) methods have been characterized as the ”gold standard” [12] in modelling the photon propagation inside human tissue. MC methods are often compared with finite-element (FE) methods [16] and are preferred when diffusion approximation becomes invalid. The main disadvantages against the FE methods are the disability of handling more complex media with curved boundaries and the need in computational resources. The development and adaptation of Graphical Processing Units in MC implementations [13] try to overcome these limitations. Similar approaches for other biomedical imaging modalities have been presented in the past [14]. The contribution of this work is the design and implementation of a simulator for MSOT, as well as combining MC and FE methods for the simulation of light propagation and their aspects through a validation with an experimental MSOT system.

E. Maneas is with the Postgraduate Program ”Information Technologies in Medicine and Biology”, Department of Informatics and Telecommunications, University of Athens, Panepistimioupolis, 15784, Athens, Greece and with the Biomedical Informatics Unit, Biomedical Research Foundation, Academy of Athens (BRFAA), S. Efessiou 4, 11527, Athens, Greece. tmaneas@di.uoa.gr

S. Tzoumas and V. Ntziachristos are with the Institute for Biological and Medical Imaging (IBMI), Helmholtz Center Munich and the Technical University of Munich, Neuherberg, D-85764, Germany. stratis.tzoumas@helmholtz-muenchen.de, v.ntziachristos@tum.de

G. Spyrou is with the Biomedical Informatics Unit, Biomedical Research Foundation, Academy of Athens (BRFAA), S. Efessiou 4, 11527, Athens, Greece. gspyrou@bioacademy.gr

II. MATERIALS AND METHODS

A. The Model

The development of an MSOT simulator includes the optical and the acoustic forward problem formulation. Finally an image reconstruction algorithm is performed to convert the simulated acoustic data to an image. Fig. 1 illustrates the steps of modelling an MSOT simulator.

1) Imaging Geometry: The geometry of the present model is depicted in Fig. 2. and is modelled in an appropriate way for small animal imaging dimensions. The detector was comprised of 64 equidistant elements, covering an angle of 172^0 and was cylindrically focused on the plane of imaged object. The focal distance between the center of the detector and the phantom's center was $4cm$.

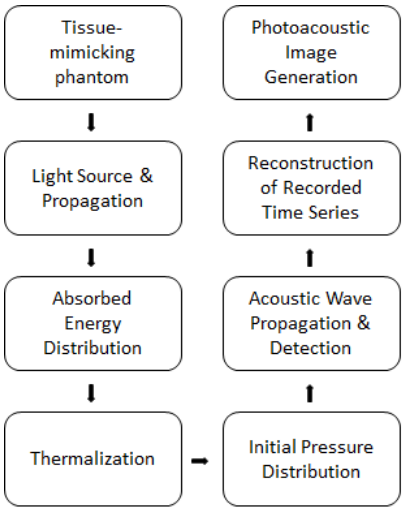

Fig. 1: Flowchart of the development of an MSOT simulator

978-1-4799-3163-7/13/$31.00 ©2013 IEEE

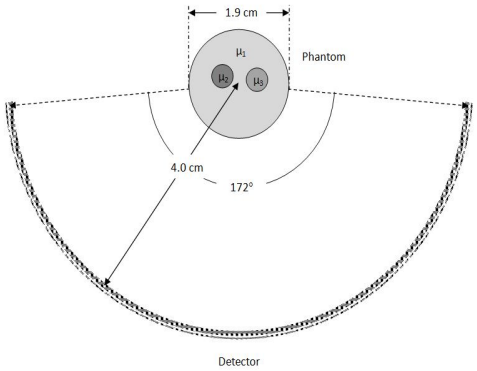

Fig. 2: Schematic of Simulation Geometry in 2D.

Also, for light source, a laser beam splitted in 10 fiber bundles was used providing uniform illumination of the imaged object. The radius of each fiber bundles' beam assumed to be 0.4 cm. These specifications were in agreement with the real-time MSOT experimental setup, described in detail in [9],[10].

2) Optics: The first step of the simulation's path is the definition of the phantom containing the absorbers (endogenous chromophores or contrast agents) as well as the light source setup.

The whole modality is submerged in a water bath. For this purpose, we used a Monte Carlo Model of steady-state light propagation in multi-layered tissues, named *MCML* [12], to describe a water layer and then to obtain the photons fluence inside this layer. Setting up the simulation, we specified this layer in a 2D grid in cylindrical coordinates with the parameters: layer's thickness, refractive index n, absorption coefficient μ_a, scattering coefficient μ_s and anisotropy factor g.

Due to the fact that the photon fluence's output of the *MCML* is based on a pencil beam, the fluence was convolved [15] with a beam with Gaussian profile and radius such that mentioned before. From this simulation, we used the fluence inside this water layer and obtained its value at the boundaries of the imaged phantom by rotating the phantom in 10 different angles, covering 360^0. The final light distribution at the boundaries was the summation of these 10 fluences. With this way, we approximated the 10 fiber bundles of the experimental laser setup, providing an homogeneous light source.

The uniform illumination at the boundaries of the imaged object was used as an input to a 2D-finite element method [16] for the computation of the light propagation inside the medium under the diffusion approximation. The result was the light's fluence, F, through the illuminated phantom.

Finishing the modelling of the optical path of optoacoustic tomography, the absorbed energy density H was calculated as the product of the absorption coefficient of the phantom (Fig. 3b) and its fluence (Fig. 3c):

$$H = \mu_\alpha F \tag{1}$$

3) Acoustics: Finally, connecting the optical path with the acoustic, the initial acoustic pressure distribution was calculated as the product of the absorbed energy density H and a thermodynamic quantity, the Grüneisen coefficient, Γ.

$$p = \Gamma H \tag{2}$$

The Grüneisen coefficient is dimensionless and assumed equal with 0.11 for water at room temperature.

For the optoacoustic signal propagation and detection we used an open source acoustics toolbox for MATLAB®, named *k-wave* [17]. For the ultrasonic wave propagation in a homogeneous fluid medium, *k-wave* solves a coupled first-order system of equations:

$$\frac{\partial \mathbf{u}}{\partial t} = -\frac{1}{\rho_0}\nabla p, \tag{3}$$

$$\frac{\partial \rho}{\partial t} = -\frac{\rho_0}{\nabla}\cdot \mathbf{u}, \tag{4}$$

$$p = c_0^2 \rho, \tag{5}$$

where u is the acoustic particle velocity, p is the acoustic pressure, ρ is the acoustic density, ρ_0 is the ambient density, and c_0 is the isentropic sound speed. These equations are related to the momentum conservation (3), mass conservation (4) and pressure-density relation (5) respectively and assume that the background medium is isotropic. Their combination results in the common second-order wave equation:

$$\nabla^2 p - \frac{1}{c_0^2}\frac{\partial^2 p}{\partial t^2} = 0 \tag{6}$$

For the recording of the propagated ultrasonic waves, a detector with its specifications mentioned in previous part was designed in *k-wave* in 2D. The sound speed of the imaged medium was assumed constant and equal with $c_0 = 1535 m/s$, comprising a value for a tissue-mimicking phantom.

4) Image Reconstruction: As a final step, the recorded pressure time series were reconstructed with a linear model-based inversion [18], in order to obtain the photoacoustic image. Model-based tomographic reconstruction is based on a explicit discrete relation between the simulated projections and the phantom. It can be written in matrix form as:

$$p = Mz, \tag{7}$$

where $p = [p_1, p_2, \ldots, p_N]^T$ represents the acquired data, $z = [z_1, z_2, \ldots, z_M]^T$ is the image values over a predetermined grid and M is the *NxM* model-matrix. The model-matrix does not depend on the imaged object and is generated for a given MSOT system and its specific acquisition geometry and also its image grid.

The inversion of (7) performed with least-square error minimization:

$$z_{sol} = \arg\min_z \|p - Mz\|^2, \tag{8}$$

where $\|\cdot\|$ is a l_2 norm and solved using the LSQR [19] algorithm with Tikhonov regularization. A detailed explanation of this image reconstruction methodology is presented in [18].

B. Validation

In order to validate the simulation model, we used reconstructed optoacoustic images of an experimental phantom as a reference to design a phantom for the input to the simulation path.

1) Experimental Setup: A cylindrical phantom consisted of a solution of water, agar and intralipid 1% was used, including three different absorbers (ink) in three different areas. The absorption values were measured using a photospectrometer as $0.23, 0.69, 0.46 cm^{-1}$ respectively. The diameter of the experimental phantom was $1.9cm$ and the excitation wavelength of the laser was determined at $740nm$.

2) Simulation Setup: A simulated phantom was created in agreement with the absorption coefficients of the experimental phantom and the position of the absorbers. The absorption was assumed homogeneous in each absorber and the reduced scattering coefficient was assumed constant through the phantom and equal with $\mu_s' = 10 cm^{-1}$. The absorption coefficient value for the specific wavelength for the optical pathway, was obtained from [20]. The scattering coefficient and the anisotropy factor values were determined to obtain the predefined reduced scattering coefficient μ_s', according to $\mu_s' = \mu_s(1-g)$.

III. RESULTS

Fig. 3a depicts the photon's fluence for a laser beam with Gaussian profile and diameter 0.8 cm. The absorption coefficient map of the imaged phantom is illustrated in Fig. 3b.

Fig. 3c illustrates the solution of the Finite Element Method of the homogeneous light distribution inside the phantom provided from multiple angle illumination.

The initial acoustic pressure distribution used as an input into the *k-wave* toolbox is depicted in Fig. 3d.

Fig. 4a and Fig. 4b present the reconstructed image from experimental and simulated data respectively, both obtained with the same image reconstruction algorithm. Fig. 4c shows a validation profile plot from the horizontal cross sections between experimental and simulated reconstructed images respectively.

IV. CONCLUSIONS AND DISCUSSION

We have developed and presented a simulator for multispectral optoacoustic tomography capable to generate MSOT images. In the first effort for validation the generated images are in agreement with the experimental ones although the absorption coefficient between the absorbing circular regions and the background was less than one order of magnitude.

Simulating the optical and acoustic phenomena in concert facilitates the direct and easy comparison with experimental data, providing better understanding of optical (light fluence)

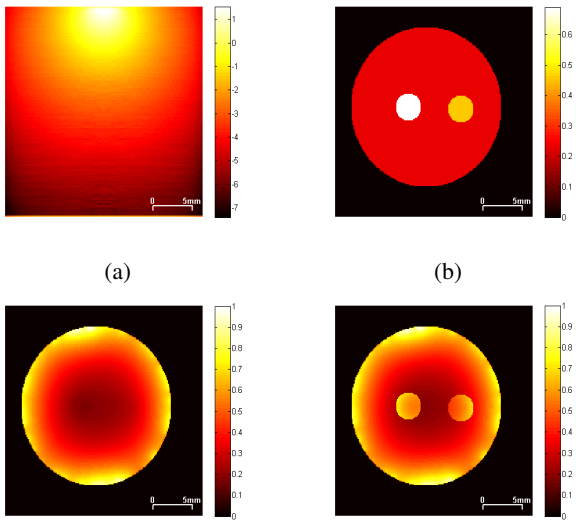

(a) (b) (c) (d)

Fig. 3: a) Photons fluence over a laser with Gaussian beam (log. scale), b) Phantom's absorption coefficients, c) Light's fluence distribution and d) Initial pressure distribution.

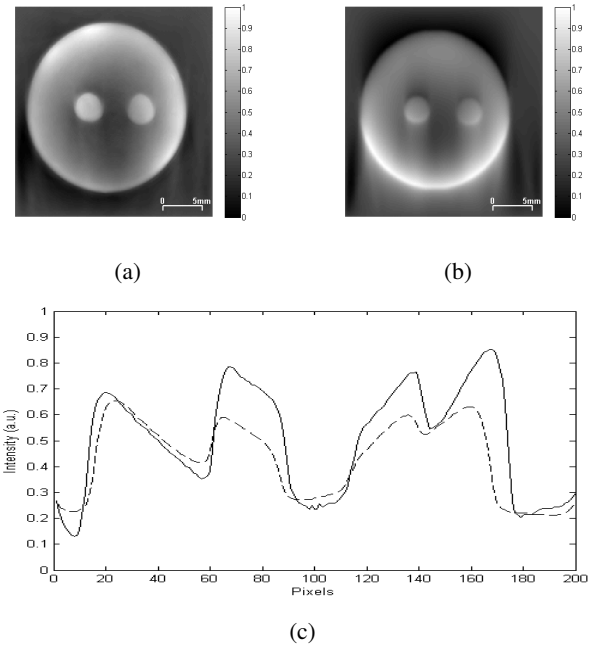

(a) (b) (c)

Fig. 4: Reconstructed a) experimental (solid line) and c) simulated (dashed line) image in arbitrary units after normalization with their horizontal cross sections c) respectively.

and acoustic (ultrasound dispersion and scattering) phenomena that are present in experimental tissue imaging.

Despite the fact that the basic phenomena are taken into account, a number of additional system features, i.e. the sensitivity field and spatial impulse response of the ultrasound sensors can largely affect the image intensity in different areas making the simulations deviate from experimental reality.

Our future work will include optimizations in the presented 2D model as well as its expansion in the full 3D space including a number of such additional system features. Also, in-silico experimentations concerning image acquisition with different geometries will be performed to exploit the capabilities of the simulator.

REFERENCES

[1] R. A. Kruger, W. L. Kiser, D. R. Reinecke, G. A. Kruger, and K. D. Miller, Thermoacoustic molecular imaging of small animals, *Mol. Imaging*, vol. 2, no. 2, 2003, pp. 113-123.

[2] X. Wang, Y. Pang, G. Ku, X. Xie, G. Stoica, and L. V. Wang, Noninvasive laser-induced photoacoustic tomography for structural and functional in vivo imaging of the brain, *Nat. Biotechnol.*, vol. 21, no. 7, 2003, pp. 803-806.

[3] V. Ntziachristos, J. Ripoll, L. V. Wang, and R. Weissleder, Looking and listening to light: the evolution of whole-body photonic imaging, *Nat. Biotechnol.*, vol. 23, no. 3, 2005, pp. 331-320.

[4] V. Ntziachristos, and D. Razansky, Molecular imaging by means of multispectral optoacoustic tomography (MSOT), *Chem. Rev.*, vol. 110, no. 5, 2010, pp. 2783-2794.

[5] P. Beard, Biomedical photoacoustic imaging, *Interface Focus*, vol. 1, no. 4, 2011, pp. 602-631.

[6] D. Razansky, M. Distel, C. Vinegoni, R. Ma, N. Perrimon, R. W. Köster, and V. Ntziachristos, Multispectral opto-acoustic tomography of deepseated fluorescent proteins in vivo, *Nat. Photon.*, vol. 3, no. 7, 2009, pp. 412-417.

[7] E. Herzog, A. Taruttis, A. Lutich, D. Razansky, and V. Ntziachristos, Optical imaging of cancer heterogeneity by means of multispectral optoacoustic tomography (MSOT), *Radiology*, vol. 263, no. 2, 2012, pp. 461-468.

[8] A. Taruttis, M. Wildgruber, K. Kosanke, N. Beziere, K. Licha, R. Haag, M. Aichler, A. Walch, E. Rummeny, and V. Ntziachristos, Multispectral optoacoustic tomography of myocardial infraction, *Photoacoustics*, vol. 1, no. 1, 2013, pp. 3-8.

[9] A. Taruttis, E. Herzog, D. Razansky, and V. Ntziachristos, Real-time imaging of cardiovascular dynamics and circulating gold nanorods with multispectral optoacoustic tomography, *Opt. Express*, vol. 18, no. 19, 2010, pp. 19592-19602.

[10] A. Buehler, E. Herzog, D. Razansky, and V. Ntziachristos, Video rate optoacoustic tomography of mouse kidney perfusion, *Opt. Lett.*, vol. 35, no. 14, 2010, pp. 2475-2477.

[11] D. Razansky, J. Baeten, and V. Ntziachristos, Sensitivity of molecular target detection by multispectral optoacoustic tomography (MSOT), *Med. Phys.*, vol. 36, no.3, 2009, pp. 939-945.

[12] L. H. Wang, S. L. Jacques, and L. Q. Zheng, MCML Monte Carlo modeling of light transport in multilayered tissues, *Comput. Meth. Prog. Bio.*, vol. 47, no. 2, 1995, pp. 131-146.

[13] Q. Fang and D. A. Boas, Monte Carlo simulation of photon migration in 3D turbid media accelerated by graphics processing, *Opt. Express*, vol. 17, 2009, pp. 20178-20190.

[14] G. Spyrou, G. Tzanakos, G. Nikiforides and G. Panayiotakis, A Monte Carlo simulation model of mammographic imaging with x-ray sources of finite dimensions, *Phys. Med. Biol.*, vol. 47, 2002, pp. 917-933.

[15] L.-H. Wang, S. L. Jacques, and L.-Q. Zheng, CONV - Convolution for responses to a finite diameter photon beam incident on multi-layered tissues, *Computer Methods and Programs in Biomedicine*, vol. 54, 1997, pp. 141-150.

[16] S.R. Arridge, M. Schweiger, M. Hiraoka, and D.T. Delpy, A finite element approach for modeling photon transport in tissue, *Med. Phys.*, vol. 20(2 Pt 1), 1993, pp. 299-309.

[17] B. E. Treeby and B. T. Cox, k-Wave: MATLAB toolbox for the simulation and reconstruction of photoacoustic wave-fields, *J. Biomed. Opt.*, vol. 15, no. 2, 2010, p. 021314.

[18] A. Rosenthal, D. Razansky, and V. Ntziachristos, Fast semi-analytical model-based acoustic inversion for quantitative optoacoustic tomography, *IEEE Trans. Med. Imaging*, vol. 29, no. 6, 2010, pp. 1275-1285.

[19] C. C. Paige and M. A. Saunders, LSQR: An algorithm for sparse linear equations and sparse least squares, *ACM Trans. Math. Software*, vol. 8, 1982, pp. 43-71.

[20] K. F. Palmer, D. Williams, Optical properties of water in the near infrared, *J. Opt. Soc. Am.*, vol. 64, 1974, pp. 1107-1110.